Supporting Information for

Solvent-Free UV Polymerization of n-Octadecyl Acrylate in Butyl Rubber: A Simple Way to Produce Tough and Smart Polymeric Materials at Ambient Temperature

Esra Su, Cigdem Bilici, Gozde Bayazit, Semra Ide, and Oguz Okay *

Department of Chemistry, Istanbul Technical University, Maslak, 34469 Istanbul, Turkey
Department of Physics Engineering and 3 Department of Nanotechnology and Nanomedicine, Hacettepe University, 06800 Beytepe, Ankara, Turkey

Table of Contents

T1: Appearance of turbidity and optimization of the reaction time.

We attempted optimization of the reaction time by monitoring UV polymerization of C18A with or without C12M in the presence of IIR by rheometry using oscillatory deformation tests. Time-sweep measurements at a frequency of 1 Hz and strain amplitude of 0.1% were conducted on a Physica MCR 302 Rheometer system (Anton Paar, Austria) equipped with an OmniCure 2000 curing system (UV light source). Figure S3 shows the reaction time dependences of *G'* (filled symbols), *G''* (open symbols), and *tan* δ (curves) of the reaction mixtures during the polymerization at 35 °C under UV light at λ = 365 nm. It is seen that gelation occurs suddenly at short reaction times and the dynamic moduli approach plateau values after around 15 min. This finding is consistent with what we observed visually: The reaction system composed of IIR, C18A (with or without C12M), and Irgacure 2959 is initially transparent while during the UV polymerization, turbidity appears first locally within ~ 1 min but then, it spreads over the whole reaction system, and the system becomes completely opaque after around 30 min. Gel fraction, DSC, and mechanical measurements conducted on the polymers isolated after reaction times of 1 and 24 h showed that they both exhibit same mechanical properties within the limits of experimental errors, less than 5% extractables in toluene, and no melting peak of C18A monomer in DCS scans. Therefore, we fixed the reaction time at 1 h.

T2: Preparation of IIR/PCxR.

Tetradecyl acrylate (C14A), hexadecyl acrylate (C16A) and hexadecyl methacrylate (C16M), all purchased from TCI Chemicals, and n-octadecyl methacrylate (C18M, Sigma-Aldrich) were used as received. Docosyl acrylate (C22A) and eicosyl acrylate (C20A) were prepared by the reaction of 1-docosanol or 1-eicosanol, respectively, with acryloyl chloride in THF in the presence of triethylamine as a catalyst, as described in the literature.[S1,S2] The purity of each batch of the synthesized monomers was checked by FTIR, and melting temperatures.

IIR/PCxR c-IPNs were prepared by melt-mixing of the reaction components IIR, CxR, and Irgacure 2959 at 80 °C followed by keeping the homogeneous mixture at 30 °C under UV light at 360 nm for 1 h. Both the IIR and Irgacure contents were fixed at 20 wt % and 0.2 wt %, respectively (both with respect to CxR). Experiments showed that IIR is insoluble in the monomers C20A and C22A. Therefore, interconnected networks of IIR with C14A, C16A, and C16M were prepared and compared with the properties of IIR/PC18A ones given in the text.

T3: Preparation and molecular weight determination of PC18A.

PC18A was prepared by UV polymerization of C18A under the same experimental condition as the c-IPNs but in the absence of IIR. After 5 min of the reaction time, samples were transferred into toluene and then the polymer was precipitated into an excess of ethanol. After washing several times with ethanol, PC18A was dried under vacuum to constant weight. The molecular weight of PC18A was determined by gel permeation chromatography (GPC) measurements on an Agilent instrument (Model 1100) consisting of a pump, refractive index, and UV detectors. Four Waters Styragel columns (HR 5E, HR 4E, HR 3, HR 2), (4.6 mm internal diameter, 300 mm length, packed with 5 μm particles) were used in series. The effective molecular weight ranges were 2000–4000000, 50–100000, 500–30000, and 500–20000 $g \cdot mol^{-1}$, respectively. THF was used as eluent at a flow rate of 0.3 $mL \cdot min^{-1}$ at 30 °C, and toluene was used as an internal standard. The molecular weight of PC18A was calculated on the basis of linear polystyrene standards (Polymer Laboratories).

Table S1.
Melting (T_m) and crystallization temperatures (T_{cry}), crystallinity fraction f_{cry}, and tensile mechanical properties of IIR/PC18A-C12M. [a]

IIR wt %	x_{C12M}	T_m / °C	T_{cry} / °C	f_{cry}	E / MPa	W / MJ m^{-3}	ε_f %
20	0	51 (2)	38.8 (0.1)	0.24	34 (2)	1.9 (0.1)	72 (6)
20	0.10	48 (1)	40.4 (0.2)	0.21	25 (3)	4.8 (0.5)	186 (12)
20	0.20	47 (1)	39.3 (0.2)	0.15	20 (3)	7.7 (1)	288 (8)
20	0.30	47 (1)	38.5 (0.5)	0.10	11 (1)	8.8 (1)	322 (28)
20	0.40	46.2 (0.5)	37.3 (0.4)	0.06	6.2 (0.8)	18 (2)	660 (63)
20	0.50	45.7 (0.4)	37.0 (0.3)	0.016	1.9 (0.2)	8.9 (0.9)	773 (22)

[a] Standard deviations are given in parentheses. For f_{cry}, they are smaller than 5%. For c-IPNs with a C12M content between 0 and 10 mol%, T_m, T_{cry}, and f_{cry} are 51±2 °C, 39±1 °C, and 0.24±0.01, respectively.

Table S2.
Healing efficiencies ε_h of c-IPNs. Healing time and temperature are 24 h and 65°C, respectively.

IIR wt%	Healing efficiency (ε_h) with respect to:		
	E	ε_f	W
20	92 ± 2 %	60 ± 2 %	62 ± 2 %
30	92 ± 3 %	88 ± 3 %	69 ± 2 %
40	97 ± 3 %	84 ± 3 %	82 ± 3 %

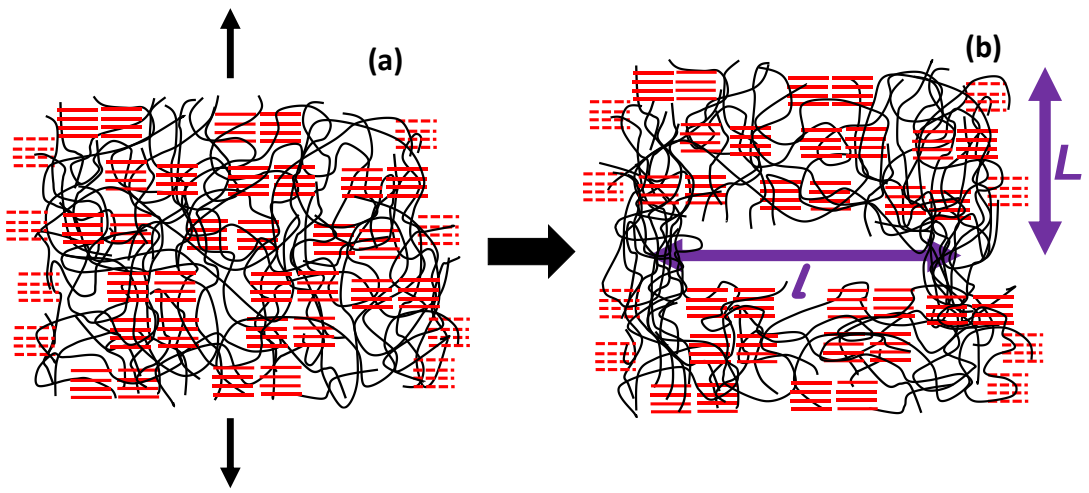

Scheme S1. Schematic presentation of crystalline domains before (a) and after application of an external force (b). Lamellar crystals and amorphous layers are shown in red and black, respectively. The external force leads to the appearance of two active tie molecules interconnecting lamellar clusters of thickness *L* with a support span length of *l*.

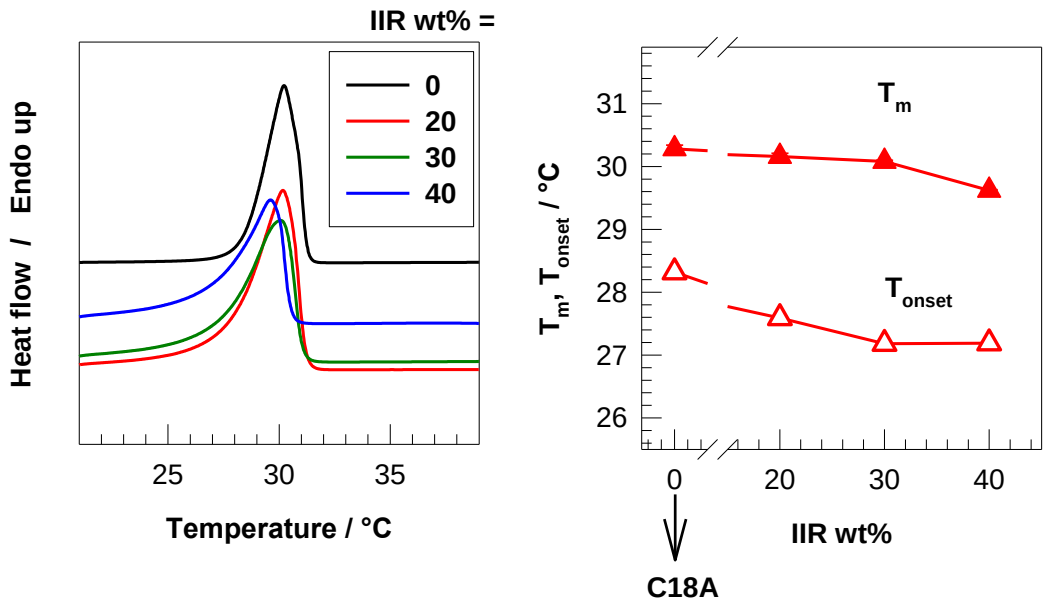

Figure S1. (a): DSC scans of IIR/C18A mixtures before polymerization at a heating rate of 1 °C·min^{-1} **(b):** The temperatures of melting (T_m) and onset of melting (T_{onset}) of IIR/C18A mixtures before polymerization plotted against IIR wt %.

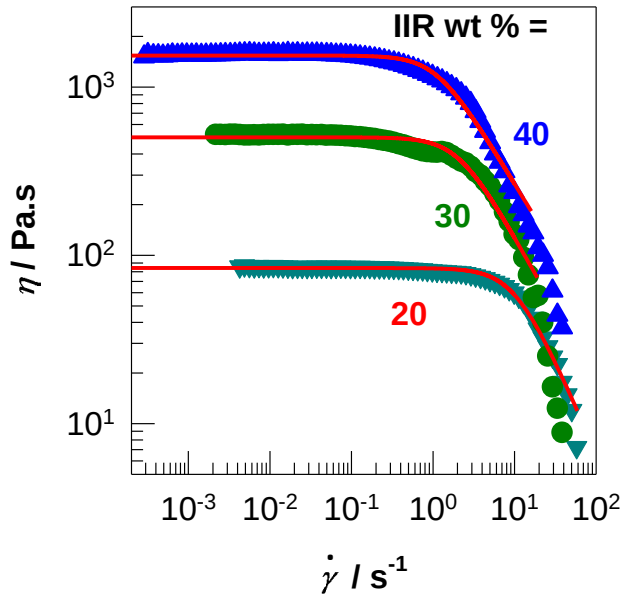

Figure S2. Shear rate (γ) dependences of the viscosities η of IIR/C18A mixtures (before polymerization) at 30 °C. Zero-shear viscosities η_o were estimated by fitting the viscosity data recorded at various shear rates to the Carreau model,[S3] $\eta(\dot{\gamma}) = \eta_o \left[1 + (\dot{\gamma}/\gamma_c)^2\right]^{-n/2}$ where γ_c is the critical shear rate and n is the shear thinning index of the shear thinning region. The best fits to the experimental data are shown by the solid red curves. For the IIR/C18A mixtures with 20, 30, and 30 wt % IIR, η_o = 84.1±0.3, 503±4, and 1540±7 Pa.s; γ_c = 10.3±0.6, 2.1±0.2, and 1.12±0.07 s^{-1}; and n = 1.11±0.07, 0.87±0.08, and 0.80±0.04, respectively.

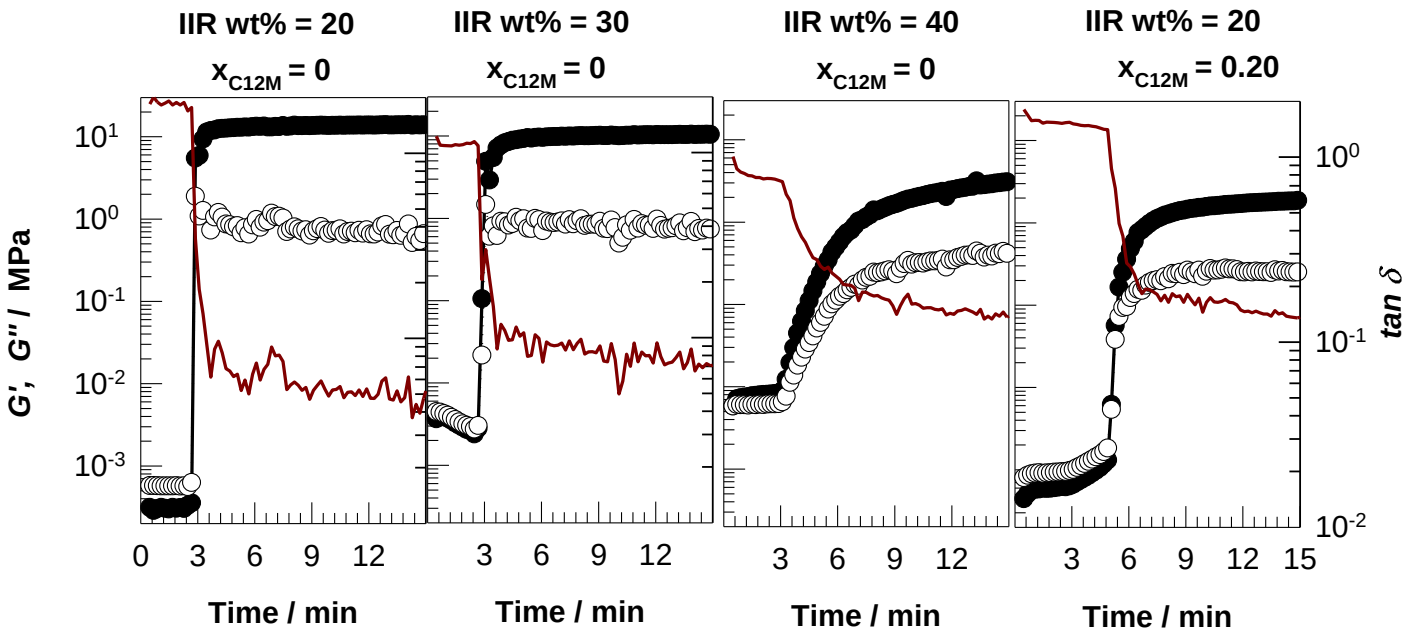

Figure S3. Reaction time dependences of *G'* (filled symbols), *G''* (open symbols), and *tan* δ (curves) of the reaction mixtures during the polymerization at 35 °C under UV light at λ = 365 nm. ω = 1 Hz. γ_o = 0.1%. The compositions of the reaction mixtures are indicated.

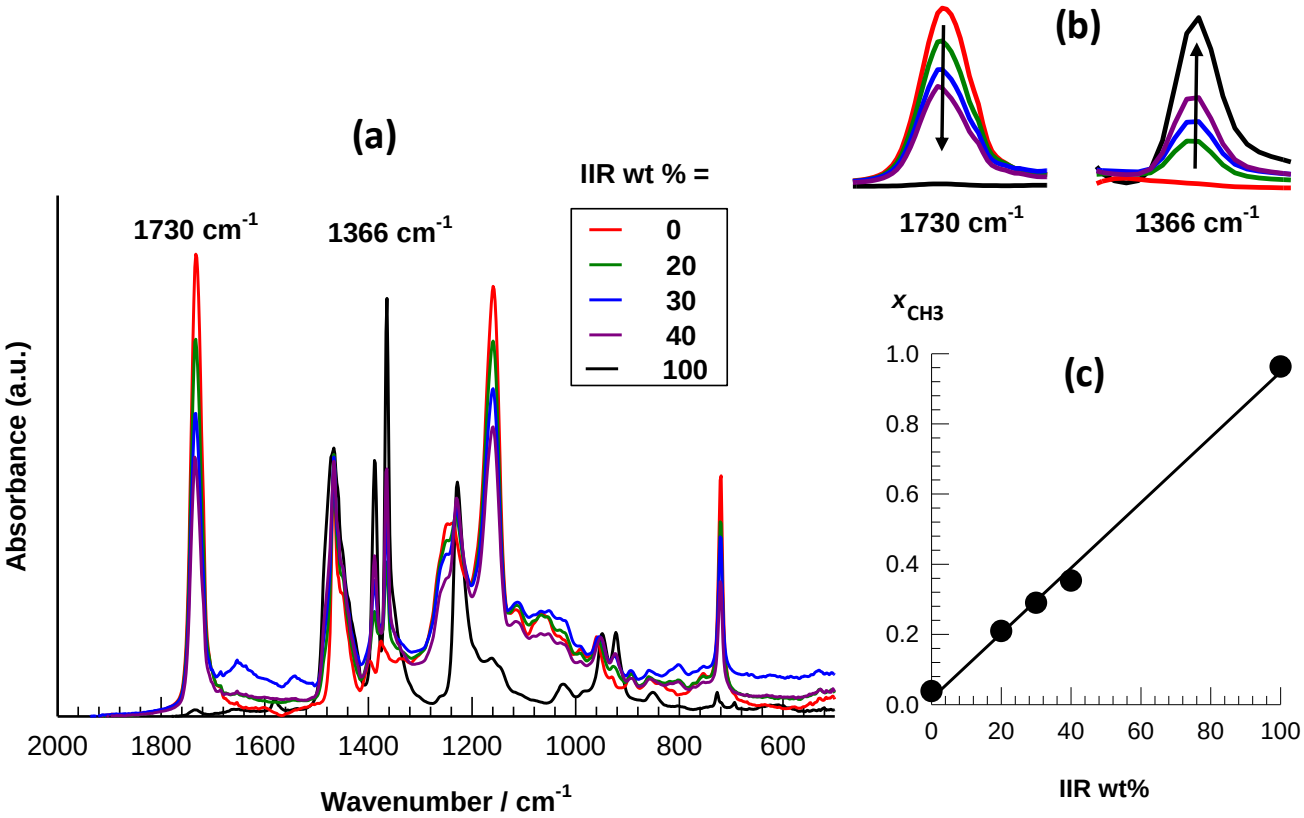

Figure S4. (a): FTIR spectra of IIR/PC18A with various IIR contents, neat IIR and PC18A. We should note that the characteristic peak of the double bonds in IIR at 1637 cm^{-1} is not visible before and after polymerization because it is very weak due to the low degree of unsaturation, i.e., 70–100 times smaller than the one observed for 1-octene.[S4] It was also reported that this signal is strongly affected by the thickness of the sample, and not reproducible for quantitative characterization.[S5] **(b):** The characteristic peaks of C18A and IIR components of c-IPNs at 1730 and 1366 cm^{-1}, respectively, corresponding to the stretching vibration of C=O in PC18A, and bending vibration of CH_3 in IIR. As indicated by the arrows, increasing IIR content also increases the intensity of the peak at 1366 cm^{-1} while that at 1730 cm^{-1} decreases. **(c):** The relative contribution of IIR component to the peak intensities (x_{CH3}) shown as a function of the IIR content of c-IPNs. x_{CH3} is given by $x_{CH3} = A_{CH3}/(A_{CH3} + A_{C=O})$, where A_{CH3} and $A_{C=O}$ are the areas under the peaks at 1366 and 1730 cm^{-1}, respectively.

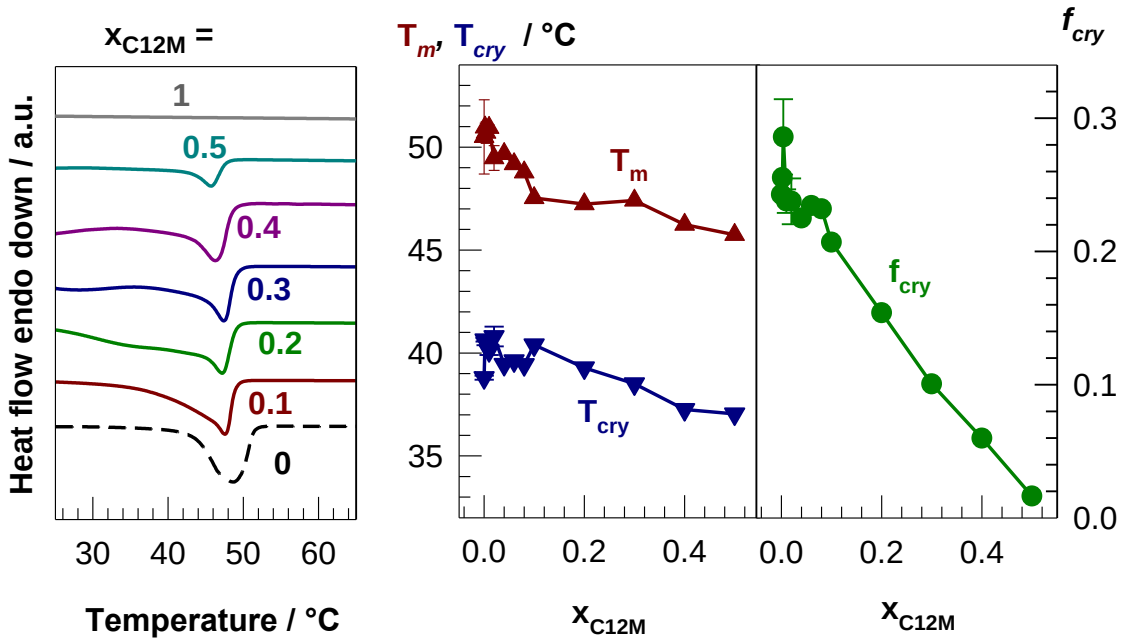

Figure S5. DSC scans, melting T_m, and recrystallization temperatures T_{cry} , and the degree of crystallinity f_{cry} of IIR/PC18A-C12M at various mole fractions of C12M (x_{C12M}). IIR = 20 wt%.

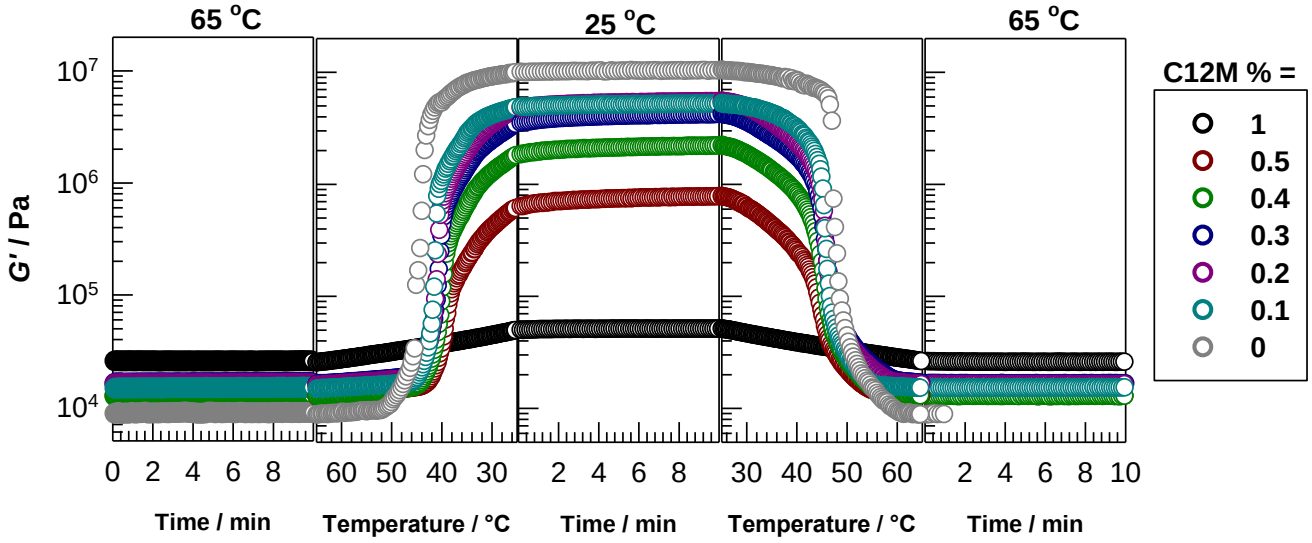

Figure S6. The variation of the storage modulus *G'* of IIR/PC18A-C12M during a thermal cycle between 65 and 25 °C. $\omega = 6.3$ rad·s^{-1}. $\gamma_0 = 0.1\%$. C12M contents are indicated.

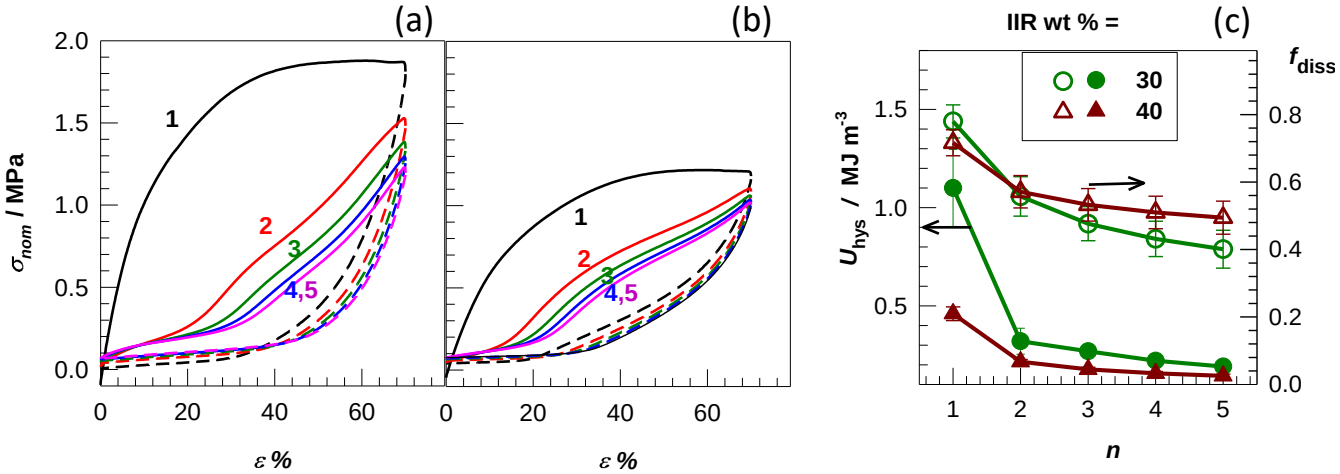

Figure S7. (a, b): Five successive tensile cycles without a waiting time between cycles up to a maximum strain (ε_{max}) of 70%. IIR = 30 (a) and 40 wt % (b). $\gamma = 5$ min^{-1}. **(c):** U_{hys} (filled symbols) and f_{diss} (open symbols) of IIR/PC18A with 30 and 40 wt % IIR plotted against the number of cycles n.

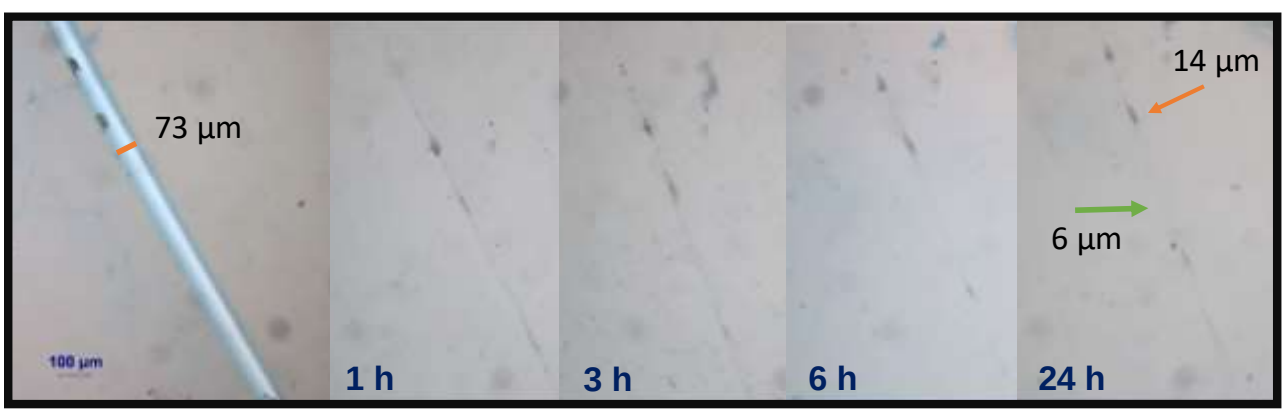

Figure S8. Optical images of the cut surface of an IIR/PC18A sample before (i) and after healing at 65 °C for various times (ii-v).

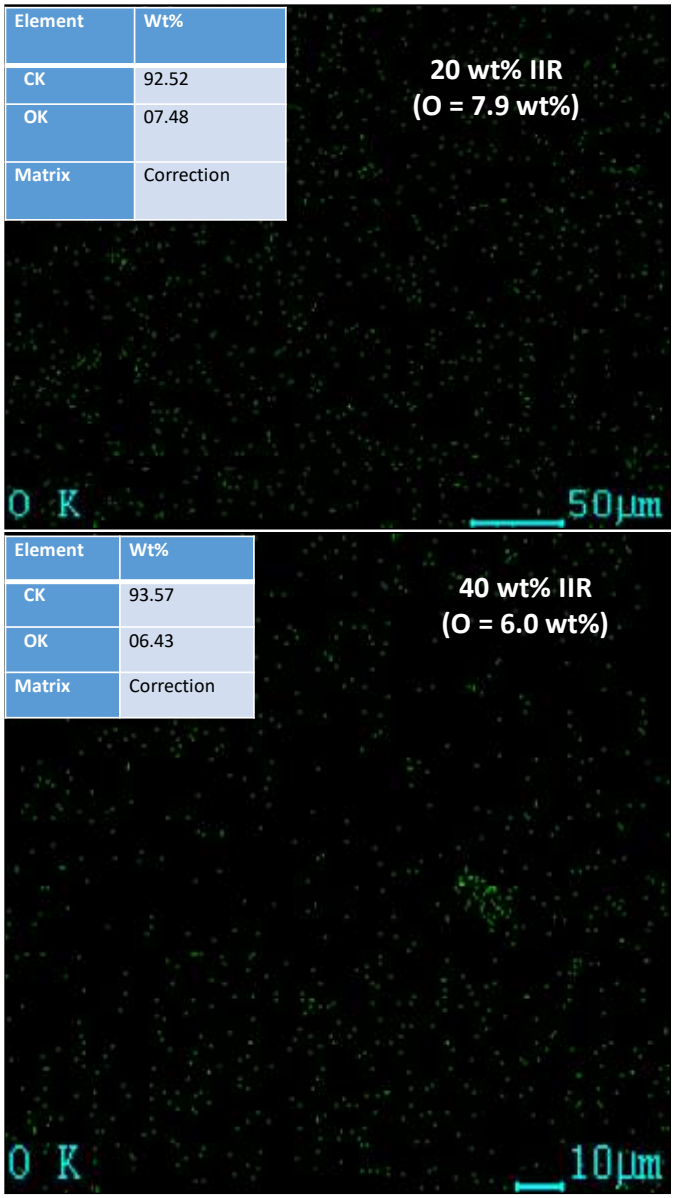

Figure S9. Elemental mapping of oxygen (green) of IIR/PC18A samples with 20 (upper panel)and 40 wt % IIR (bottom panel). The surface oxygen content of the samples from EDX analysis is 7.5 and 6.4 wt % for 20 and 40 wt % IIR, respectively, as compared to the overall oxygen contents of 7.9 to 6.0 wt%.

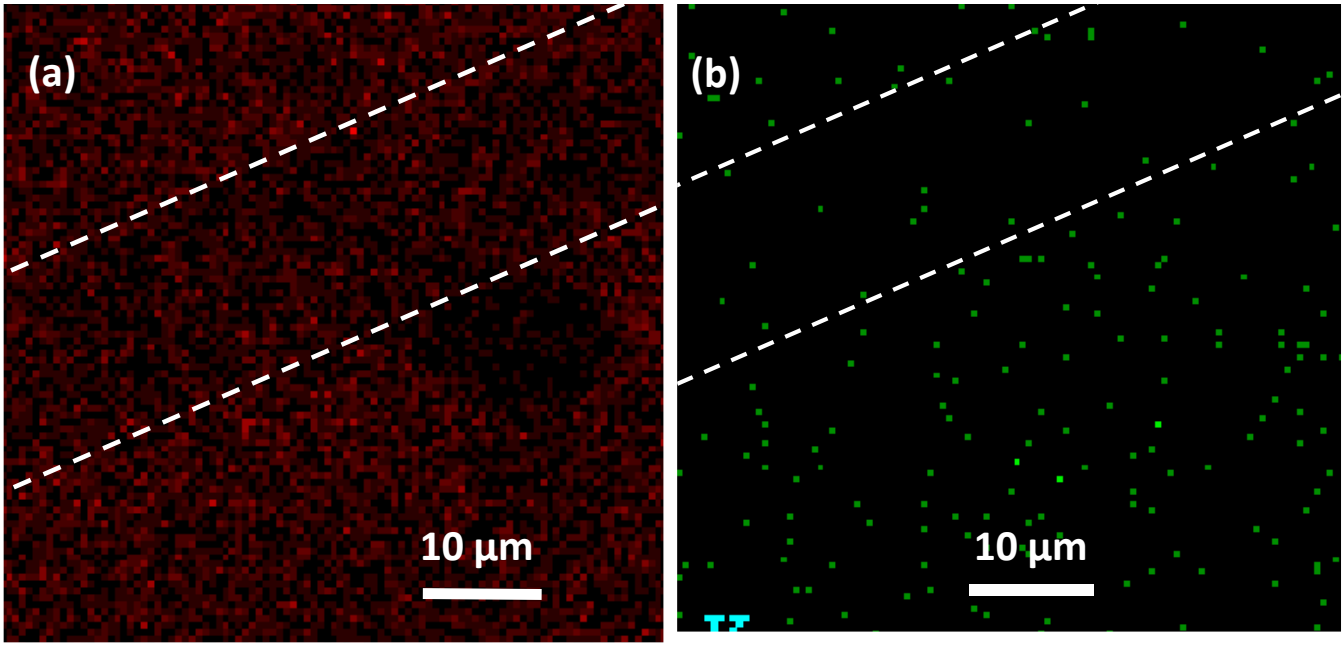

Figure S10. Elemental mapping of C (a) and O atoms (b) for an IIR/PC18A sample with 40 wt% IIR after healing at 50°C for 5 min. The parallel white lines surround the healed area.

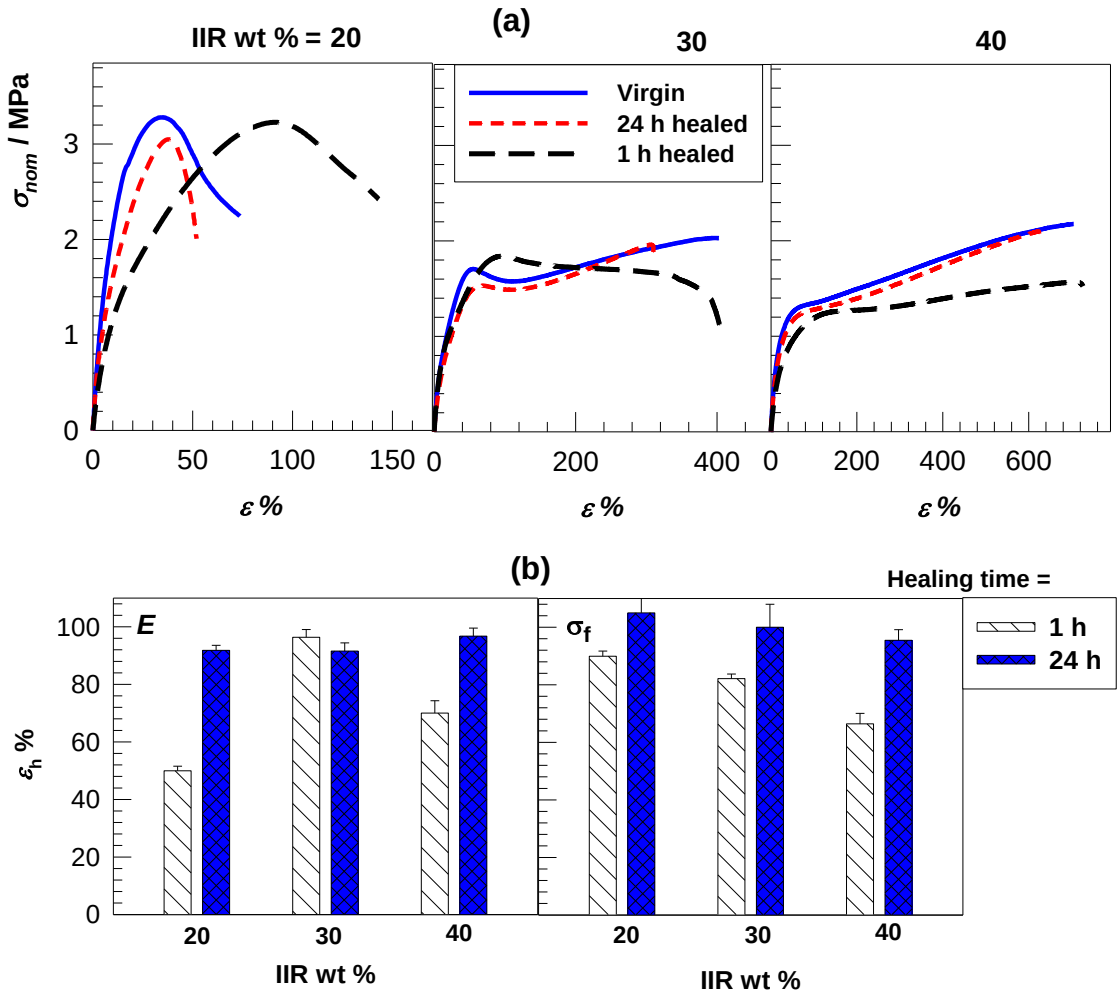

Figure S11. (a): Stress-strain curves of virgin (solid curves) and healed (dashed curves) IIR/PC18A with various IIR contents. Healing was conducted by heating at 65 °C for 1 and 24 h. **(b):** Healing efficiencies ε_h with respect to the modulus E (left), and fracture stress σ_f (right) plotted against IIR content of the c-IPNs.

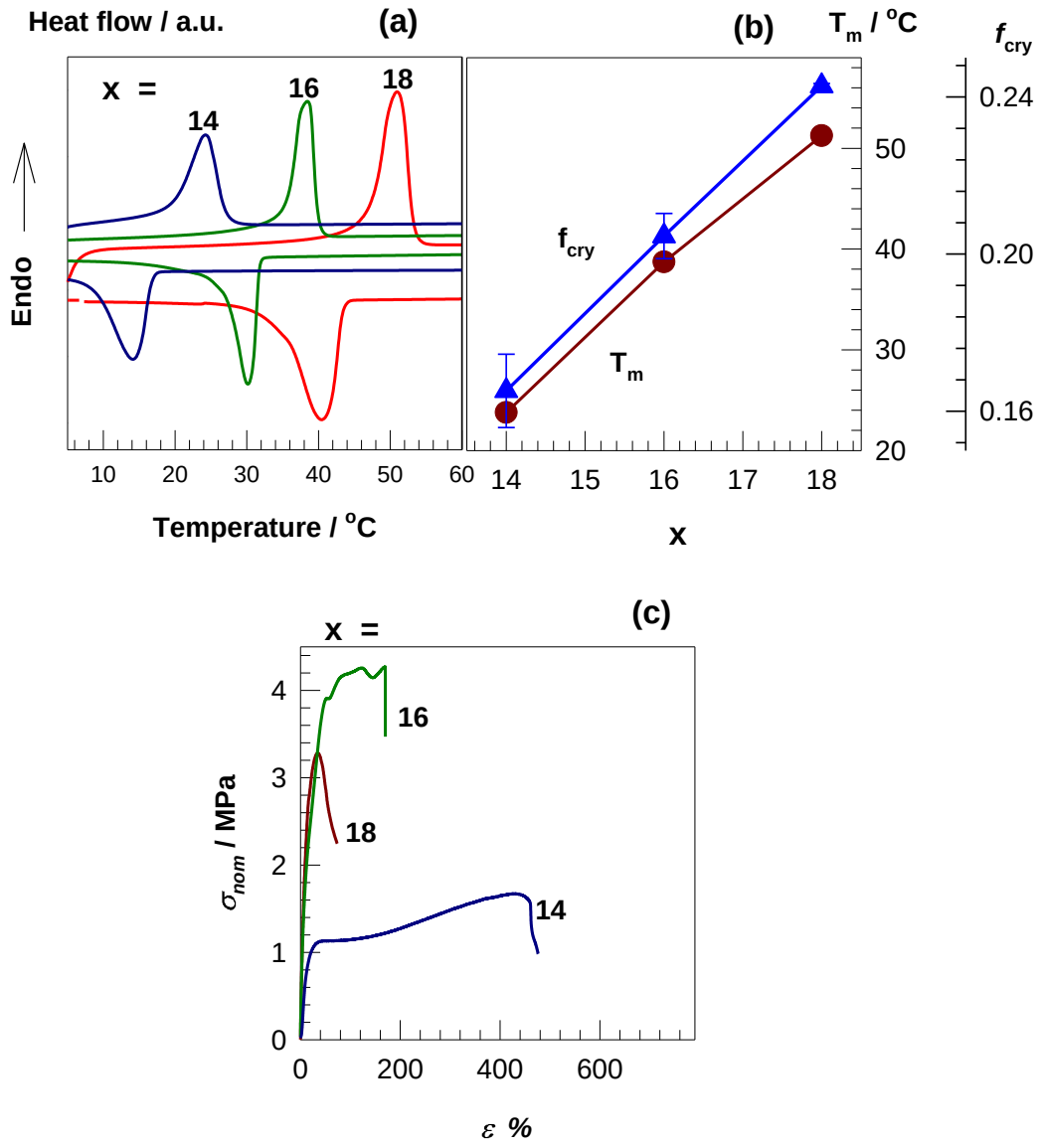

Figure S12. (a): DSC patterns of IIR/CxA with x = 14, 16, and 18. (b): The melting temperature T_m and the degree of crystallinity f_{cry} of IIR/CxA plotted against x. (c): Stress strain curves of IIR/CxA with x = 14, 16, and 18.

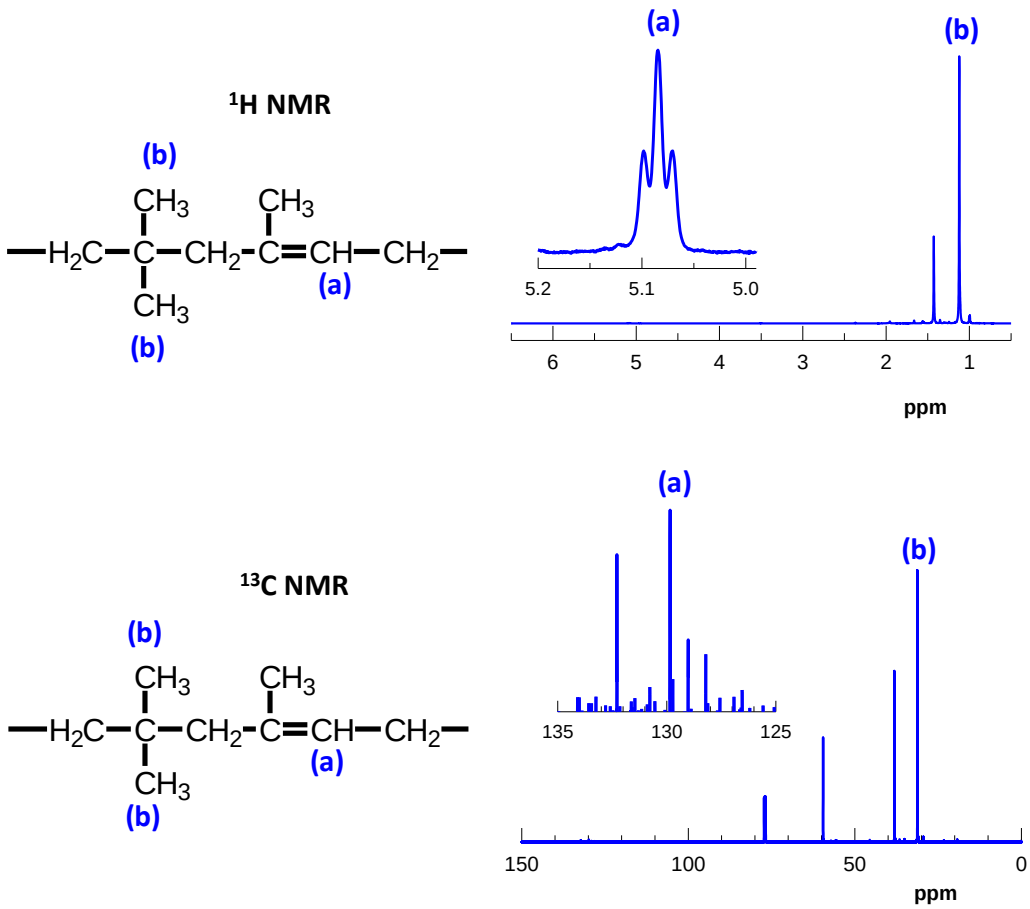

Figure S13. ^{1}H NMR (upper panel) and ^{13}C NMR spectra (bottom panel) of IIR. For the measurements, small pieces of IIR, 10-15 mg, were dissolved in 0.6 mL of deuterated chloroform ($CDCl_3$) and then, the solution was transferred in 4 mm NMR tubes. Due to the low degree of unsaturation, the peaks related to the isoprene units need to be magnified as shown in the insets to the figure. In the ^{1}H NMR spectrum, the triplet between 5.02 and 5.15 ppm denoted by (a) corresponds to methine of isoprene units whereas the peaks at 1.1 and 1.4 ppm are related to the CH_3 and CH_2 groups of IIR, respectively.[S4] The unsaturation degree was calculated using the equation,

$$\text{Unsaturation (mol\%)} = \frac{a}{a + b/6} 10^2 \qquad \text{(S1)}$$

where a is the normalized integral signal intensity of the region 5.02-5.15 ppm, and b is the same intensity at 1.1 ppm corresponding to the CH_3 groups (peak (b) in Figure S1). In the ^{13}H NMR spectrum, the signals at 130 and 31.7 ppm denoted by (a) and (b), respectively, are associated with =CH and CH_3 carbon atoms, respectively.[S6] The unsaturation degree was calculated using the equation,

$$\text{Unsaturation (mol\%)} = \frac{a}{a + b/2} 10^2 \qquad \text{(S2)}$$

where a and b are signal intensities at 130 and 31.7 ppm, respectively. The degree of unsaturation of IIR calculated as 1.9±0.1 and 1.6±0.3 mol% from ^{1}H NMR and ^{13}C NMR measurements, respectively, was reported as 1.7±0.2 mol% in the text.

References

(S1) Miyazaki, T.; Kaneko, T.; Gong, J. P.; Osada, Y. Effects of carboxyls attached at alkyl side chain ends on the lamellar structure of hydrogels. *Macromolecules* **2001**, 34, 6024-6028.

(S2) Tuncaboylu, D. C.; Argun, A.; Sahin, M.; Sari, M.; Okay, O. Structure optimization of self-healing hydrogels formed via hydrophobic interactions. *Polymer* **2012**, 53, 5513-5522.

(S3) Carreau, P. J. Rheological equations from molecular network theories. *Trans. Soc. Rheol.* **1972**, 16, 99-127.

(S4) Vitiello, R.; Tesser, R.; Turco, E.; Santacesaria, G.; Compagnone, M. Di Serio. A critical review on analytical methods and characterization of butyl and bromobutyl rubber. *Int. J. Polym Anal. Ch*. **2017**, 22, 348-360.

(S5) Cheng, D. M.; Gardner, I. J.; Wang, H. C.; Frederick, C. B.; Dekmezian, A. H.; Hous, P. Spectroscopic studies of the structures of butyl and bromobutyl rubbers. *Rubber Chem. Technol.* **1990**, 63, 265–275.

(S6) Chu, C. Y.; Vukov, R. Determination of the structure of butyl Rubber by NMR spectroscopy. *Macromolecules* **1985**, 18, 1423-1430.